Progress In Electromagnetics Research, Vol. 136, 211–223, 2013

DESIGN OF A MINIATURIZED DUAL-BAND DOUBLE-FOLDED SUBSTRATE INTEGRATED WAVEGUIDE BANDPASS FILTER WITH CONTROLLABLE BANDWIDTHS

Qiaoli Zhang[1, *], Bingzhong Wang[1], Wenyan Yin[2], and Linsheng Wu[3]

[1]Institute of Applied Physics, School of Physical Electronics, University of Electronic Science and Technology of China (UESTC), Chengdu 610054, China

[2]Centre for Optical and Electromagnetic Research, State Key Lab of MOI, Zhejiang University, Hangzhou 310058, China

[3]Key Laboratory of Ministry of Education of Design and EMC of High-Speed Electronic Systems, Shanghai Jiao Tong University, Shanghai 200240, China

Abstract—One miniaturized multilayer dual-band bandpass filter (BPF) is developed using standard low temperature co-fired ceramic (LTCC) technology. The filter makes use of four double-folded substrate integrated waveguide (SIW) resonators. Two sets of coupling paths between the source and load are implemented to generate dual-band responses. Utilizing this method, the two passbands can operate at independent frequencies and the bandwidth can be easily controlled. High isolation is obtained between two passbands, and two pairs of transmission zeros close to the passband edges are generated by source-load coupling, resulting in high skirt-selectivity. Good agreement between the simulated and measured results of the filter sample is obtained, with its high electrical performance validated.

Received 14 December 2012, Accepted 10 January 2013, Scheduled 17 January 2013

* Corresponding author: Qiaoli Zhang (qlzhang@uestc.edu.cn).

1. INTRODUCTION

Recently, SIWs, formed by placing two rows of metallic via-holes, either in printed circuit board (PCB) or in LTCC substrate, have been widely studied for microwave and millimeter wave applications. Due to their advantages of high Q-factor, high power handling capability, low loss, low cost, and compact size [1], there have been a great number of applications in various circuit designs based on SIW structures, especially in compact filter designs [2–6]. The SIW filters stand on a vantage point not only for the advantages of traditional waveguide filters and easy integration with planar circuits, but also because the coupling coefficients can be controlled accurately at each band by slots or via spacing. Since resonators are the basic components of filters, several approaches for design of miniaturized waveguide resonators have been developed. One of the practical methods is double-folded waveguide resonator [7, 8]. The concept of combining SIW and folded waveguide technologies has been introduced for further reducing the SIW width [9]. The improved structure has only half the width of its equivalent SIW structure, but retains the similar cutoff and propagation characteristics [10]. Thus, folded SIW cavity is a good choice for the miniaturized filter designs [9–15].

On the other hand, we would like to indicate that dual-band BPFs are very useful for multiband wireless communications. In the past years, many researches have been carried out for developing new dual-band BPFs [16–25]. One of the simplest methods is by connecting two different passband BPFs in parallel to obtain the dual-band characteristics [18–21], and it has the advantage of two controllable bandwidths. Dual-band resonators such as stepped-impedance resonators (SIRs) are suitable for the dual-band filter designs, because the ratio of the fundamental frequency and the higher order mode frequencies can be controlled and the spurious frequency responses can be utilized to create second passband [22–25]. However, most of them are focused on the realization of microstrip or coplanar waveguide dual-band BPFs and fabricated using PCB technology. More recently, some dual-band SIW filters have already been proposed by using inverter coupled resonator sections or taking advantage of the existence of multiple cavity modes, but the realization of dual-band filters using compact SIW structures is not widely researched until now [26–28].

In this paper, a dual-band BPF is designed by using four double-folded SIW resonators, and fabricated using standard LTCC technology. Two coupling paths are utilized to provide two independent signal paths. It is found that the center frequency and

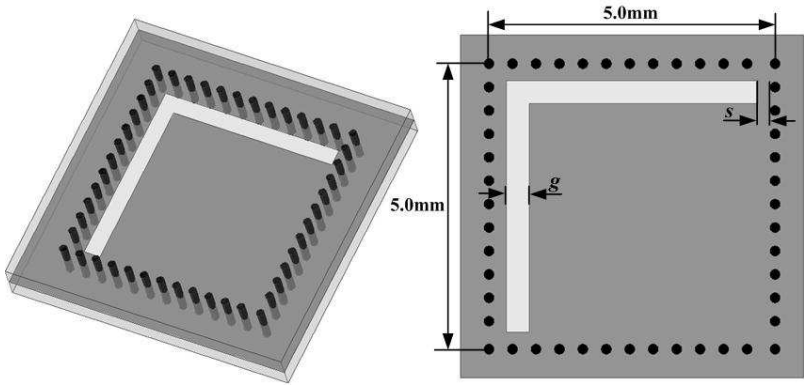

Figure 1. (a) 3D geometry of double-folded SIW resonator, and (b) configuration of the central metal plane.

bandwidth of one passband can be easily tuned, while the other one are kept unchanged. In addition, source-load coupling is also employed to create four transmission zeros near the passbands edges, resulting in high skirt selectivity. Based on the idea, a filter sample is implemented. The measured results exhibit good agreement with the full-wave simulation results, and its high electrical performance of the filter is validated.

2. ANALYSIS AND DESIGN

2.1. FSIW Resonator

Figure 1 shows the geometry of a double-folded SIW resonator, where the width and length of the resonator are both set to 5.0 mm, g is the width of the L-shaped slot in the central metal plane, and s is the distance between the slot and metallic via-holes. Since the rectangular TE_{101} waveguide resonator is folded along the thickness direction twice, there is about 50% reduction in the overall volume if the thickness of two dielectric layers is taken into consideration.

Since the width and length of double-folded SIW resonator are almost half the size of a SIW resonator, it has approximately the same resonant frequency as the SIW resonator. However, the L-shaped slot has significant effect on the resonant frequency. Figure 2 shows the resonant frequencies versus slot width g and distance s. It is observed that resonant frequency increases with increasing g or s. In our study, we would like to set both g and s as 0.3 mm.

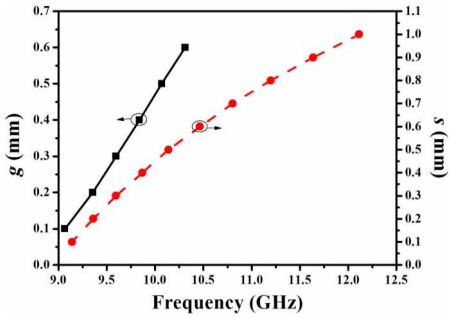

Figure 2. The resonant frequencies of a double-folded SIW resonator as functions of g and s.

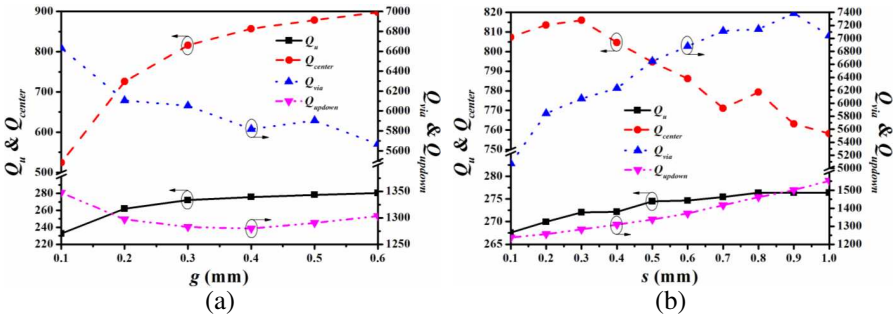

Figure 3. The Q-factors of a double-folded SIW resonator as functions of (a) g, and (b) s.

The double-folded SIW resonator can maintain the resonant modes resembling the TE_{101} mode in a conventional waveguide resonator and thus has a similar good Q property. As the radiation loss can be neglected, the in-band insertion loss of the double-folded SIW resonator is determined by the unloaded Q-factor Q_u, which is calculated by

$$1/Q_u = 1/Q_c + 1/Q_d = 1/Q_{updown} + 1/Q_{center} + 1/Q_{via} + 1/Q_d \quad (1)$$

where Q_c and Q_d are the Q-factors due to the conductor and dielectric loss, respectively; Q_{updown}, Q_{center} and Q_{via} are the Q-factors corresponding to the conductor loss in the top and bottom metal plane, center metal plane, and metallic via-holes, respectively. Using full-wave EM simulator-Ansoft HFSS, the estimated Q-factors of double-folded SIW resonator can be extracted. Figure 3 shows the values of Q_u, Q_{updown}, Q_{center} and Q_{via} as functions of the slot width g and the

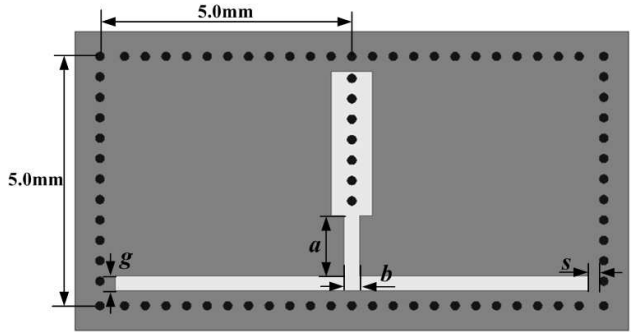

Figure 4. The configuration of the negative coupling between double-folded SIW resonators.

distances between the slots and metallic via-holes s. Q_d is not given since it does not vary with the changes of g and s. It is observed that loss introduced by the via-holes is very small and can be neglected. The value of Q_{center} increases with increasing g, because of the reduction of the conductor loss of the slots; but for increasing s, the curve has an opposite trend. Since the surface current on the top and bottom plane will increase for wide slots, Q_{updown} decreases as slot width increases. Then, Q_u can be improved by increasing slots width g and the distance s. When both g and s are set to 0.3 mm, the extracted Q_u, Q_{updown}, Q_{center}, Q_{via} and Q_d of the double-folded SIW resonator are around 272, 1283, 816, 6005 and 667 at 9.6 GHz, respectively.

2.2. Internal Couplings

As presented in [29], the negative coupling of two double-folded SIW resonators could be realized by forming a post-wall iris combined with capacitive vanes between them since the electric field is perpendicular to the gap region. The configuration of the negative coupling is shown in Figure 4. The coupling coefficients can be controlled by the dimensions of the capacitive vanes a and the gap between them b.

The coupling coefficients are calculated by [30]

$$M = \pm \frac{f_{r2}^2 - f_{r1}^2}{f_{r2}^2 + f_{r1}^2} \tag{2}$$

where f_{r1} and f_{r2} represent the lower and higher resonant frequency, respectively. The numerical analysis can be used to determine the coupling coefficients, as shown in Figure 5. As a increases, the area of the capacitive vanes will become larger, therefore, the coupling between two double-folded SIW resonators becomes stronger. Meanwhile, the

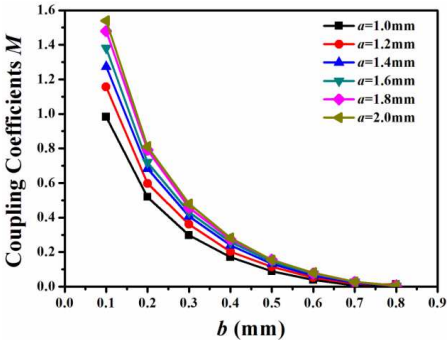

Figure 5. Negative coupling coefficients with different value of a and b.

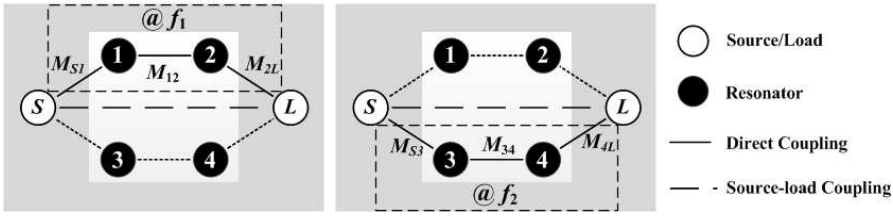

Figure 6. The coupling mechanism at (a) lower and (b) upper frequencies.

couplings coefficients decrease as the value of b increases since the electric field coupling will become weak with increasing of the gap between two capacitive vanes. Furthermore, when b increased to a certain value, the coupling coefficients will keep unchanged with increasing of a.

2.3. Filter Topology and Mechanism

Figure 6 shows the feed and coupling mechanism of the dual-band BPF based on two coupling paths. The operating frequencies and bandwidths of two passbands can be controlled independently. At lower passband, resonators 1 and 2 generate a signal path from source to load as shown in Figure 6(a). Because of non-resonance at f_1, resonators 3 and 4 almost do not affect the response of the lower passband. While at the upper passband, resonators 3 and 4 provide another signal path shown in Figure 6(b). Resonators 1 and 2 can be neglected due to their little contribution to the upper passband.

Thus, it is verified that high isolation can be obtained between the two specific passbands of the filter by using this kind of feed and coupling scheme.

A simple analysis of the network along the lines shows the loop currents, which are grouped in a vector $[I]$, are given by a matrix equation of the form [31]

$$[-jR + \Omega W + M][I] = [A][I] = -j[e], \quad j^2 = -1 \tag{3}$$

where $[R]$ is a $(n+2) \times (n+2)$ matrix with all elements zero, except for $R_{11} = R_{n+2,n+2}$. The matrix $[W]$ is the $(n+2) \times (n+2)$ identity one, except that $W_{11} = W_{n+2,n+2} = 0$. The matrix $[M]$ is the $(n+2) \times (n+2)$ coupling one, which is reciprocal and M_{ij} is frequency-independent. The coupling matrix $[M]$ is allowed to have nonzero diagonal elements M_{ii} for an asynchronously tuned filter. The excitation vector is given by $[e]^t = [1, 0, 0, \ldots, 0]$. The low-pass frequency variable $\Omega = (\omega/\omega_0 - \omega_0/\omega)/FBW$, where ω_0 and FBW are the central frequency and fractional bandwidth of the filter, respectively. Therefore, we obtain the S-parameters as [31]

$$S_{21} = -2j \left[A^{-1}\right]_{n+2,1} \tag{4}$$

$$S_{11} = 1 + 2j \left[A^{-1}\right]_{1,1} \tag{5}$$

In order to generate two transmission zeros at two sides of the passband, the product of four coupling coefficients in the coupling matrix $[M]$ should satisfy $M_{S1} \cdot M_{12} \cdot M_{2L} \cdot M_{SL} < 0$, and this means that one of the four coupling coefficients should be negative. Considering the structure symmetry, the topologies with and without source-load coupling are studied here, and the S_{21}-parameters of the topology with different internal couplings are plotted in Figure 7. It is observed that the transmission zero disappears when the source-load coupling is eliminated. As the internal coupling is negative and the source-load coupling is introduced in the topology, two pairs of transmission zeros are introduced at both upper and lower sides of the two passbands simultaneously.

2.4. Dual-band Filter Design

Based on the above topology analysis, a multilayer double-folded SIW dual-band BPF is designed in this section. The configuration of the proposed dual-band BPF is shown in Figure 8. Obviously, the center frequencies of the specific passbands are determined by the size of the double-folded SIW cavities and the value of g and s. Here, in our study, two passbands operate at 10 and 13 GHz, respectively. There are four double-folded SIW resonators denoted by 1, 2, 3 and 4, respectively.

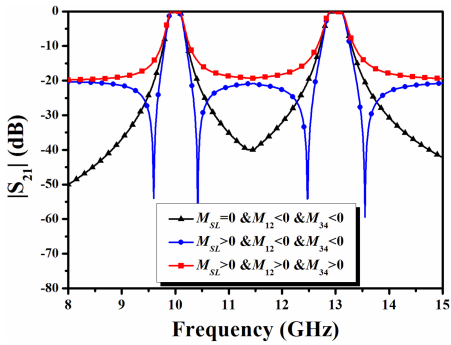

Figure 7. Transmission coefficients with different combinations of internal and source-load couplings.

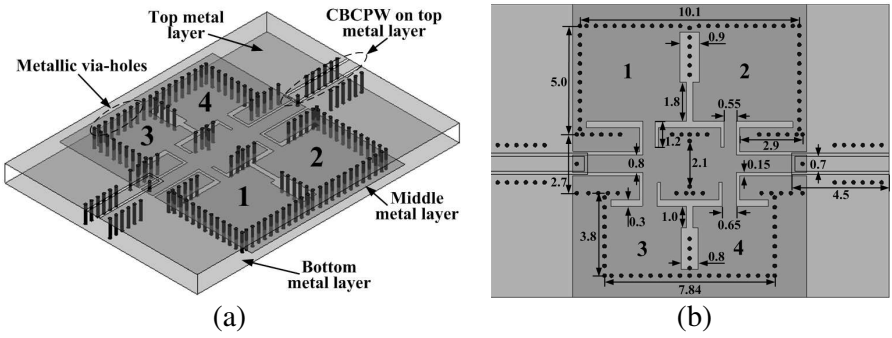

Figure 8. Proposed double-folded SIW dual-band BPFs using two coupling paths based on LTCC: (a) perspective view and (b) top view (unit: mm).

In each coupling path, two double-folded SIW resonators are coupled with each other by negative coupling, which is realized by adding two separate capacitive vanes in the gap region [29]. The internal coupling coefficient between two coupled resonators, M_{12} or M_{34} is determined by dimension of the capacitive vanes a and gap b. As shown in Figure 7, a pair of transmission zeros are located at the lower and upper side of each passband, respectively, and their relative locations are determined by adjusting the external coupling coefficients Q_e. At each specific passband, the Q_e is determined by the coupling between coplanar waveguide feed line and resonator 1 or 3, i.e., the length and width of the feed line. It is found that the external quality factors and the coupling coefficients at two specific passbands are independent once the parallel feed scheme is confirmed. This property provides high

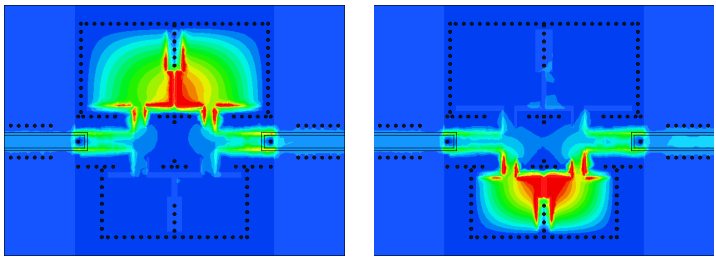

Figure 9. The electric field distributions in the multilayer dual-band double-folded SIW BPF: (a) at lower and (b) at upper frequencies.

degree of freedom to control the frequencies and bandwidths of both passbands, respectively. The source-load coupling is magnetic coupling generated by employing a conventional inductive window between two SIW sections. The coupling strength can be conveniently adjusted by controlling the window size. Figure 9 shows the inner electric fields of this multilayer dual-band filter, and there is no mutual coupling between two signal paths.

3. RESULTS AND DISCUSSIONS

The multilayer double-folded SIW filter prototype shown in Figure 8 is fabricated in a LTCC Ferro-A6 substrate, which has its permittivity of 5.9, its loss tangent of 0.15%, and its uniform dielectric layer thickness of 0.096 mm. Its geometrical parameters are depicted in Figure 8. Figure 10 shows the photo of the fabricated filter sample. Each double-folded SIW resonator consists of 4-layer substrate. All metallic vias have a diameter $d_{via} = 0.18$ mm, and their spacing is $p_{via} = 0.43$ mm. The feedlines of the multilayer structure are strip lines, and for our measurement, they are connected with the 50 Ω conductor-backed coplanar waveguides (CBCPWs) on the top metal plane.

The S-parameters of the filter sample is measured using the Anritsu universal test fixture 3680 K and Anritsu MS4644A vector network analyzer, with a set of coplanar ground-signal-ground (GSG) probes used for our measurement. Figure 11 shows the measured results, together with the simulated ones for comparison. Its measured central frequencies are 10.1 and 13.2 GHz, respectively. At lower passband, it has 3-dB bandwidth of 280 MHz, and the measured in-band return and insertion losses, including the loss from SMA connectors, are better than 16 dB and about 2.2 dB, respectively. Due

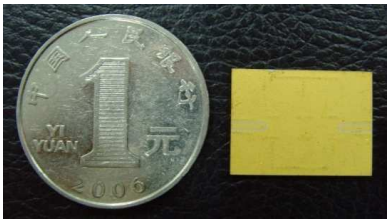

Figure 10. Photo of the fabricated multilayer dual-band double-folded SIW filter.

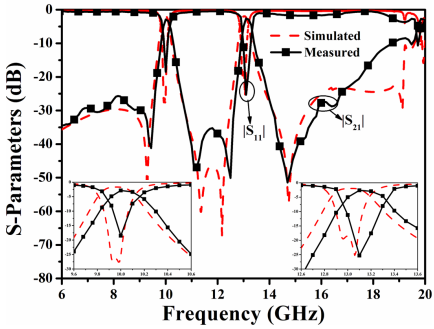

Figure 11. Measured and simulated S-parameters of the multilayer dual-band double-folded SIW filter.

to source-load coupling, there are two transmission zeros on both sides of the lower passband located at 9.52 and 11.23 GHz. The upper passband has a 3-dB bandwidth of 355 MHz. The measured in-band return and insertion losses are better than 17 dB and 2.9 dB, respectively. The two transmission zeros are located at 12.6 and 14.78 GHz. Evidently, the measured results agree well with the simulated ones obtained by commercial software HFSS, except a small frequency shift and a little discrepancy in the in-band insertion loss. This is mainly caused by the inaccuracy in the characterization of relative permittivity of LTCC and its manufacturing tolerance. In addition, the influence of the transition between a pair of GSG probes and CBCPWs will also result in the discrepancy in the simulated and measured in-band insertion losses.

4. CONCLUSION

A miniaturized multilayer dual-band double-folded SIW BPF is developed using standard LTCC fabrication technology. Two sets of coupling paths between the source and load are adopted so as to achieve dual-band performances. Using this configuration, the operating frequencies of both passbands can be tuned independently, and their bandwidths can be controlled effectively. Four transmission zeros are created to improve the selectivity of the filter due to the source-load coupling. The good RF performance is validated by its simulated as well as measured results. Compared with the dual-band bandpass filter implemented with single-layer conventional SIW

structures, the size reduction of this multilayer double-folded BPF is about 75%, implying more compact design. Furthermore, the proposed dual-band BPF is easy for fabrication, convenient for integration with planar circuits, and attractive for many applications.

ACKNOWLEDGMENT

This work has been supported by the National Basic Research Program under Grant of China (No. 2009CB320204) and the Fundamental Research Funds for the Central Universities (No. ZYGX2012J051).

REFERENCES

1. Piloto, A., K. Leahy, B. Flanick, and K. A. Zaki, "Waveguide filters having a layered dielectric structures," U.S. Patent 5382931, 1995.
2. Deslandes, D. and K. Wu, "Single-substrate integration technique of planar circuits and waveguide filters," *IEEE Trans. on Microw. Theory and Tech.*, Vol. 51, No. 2, 593–596, 2003.
3. Zhang, Z. G., Y. Fan, Y. J. Cheng, and Y.-H. Zhang, "A novel multilayer dual-mode substrate integrated waveguide complementary filter with circular and elliptic cavities (SICC and SIEC)," *Progress In Electromagnetics Research*, Vol. 127, 173–188, 2012.
4. Xu, Z. Q., Y. Shi, P. Wang, J. X. Liao, and X. B. Wei, "Substrate integrated waveguide (SIW) filter with hexagonal resonator," *Journal of Electromagnetic Waves and Applications*, Vol. 26, Nos. 11–12, 1521–1527, 2012.
5. Cheng, Y. J., "Substrate integrated waveguide frequency-agile slot antenna and its multibeam application," *Progress In Electromagnetics Research*, Vol. 130, 153–168, 2012.
6. Zhang, Q.-L., W.-Y. Yin, S. He, and L.-S. Wu, "Evanescent-mode substrate integrated waveguide (SIW) filters implemented with complementary split ring resonators," *Progress In Electromagnetics Research*, Vol. 111, 419–432, 2011.
7. Chen, G. L., T. L. Owens, and J. H. Whealton, "Theoretical study of the folded waveguide," *IEEE Trans. on Plasma Sci.*, Vol. 16, No. 2, 305–308, 1998.
8. Hong, J. S., "Compact folded waveguide resonator," *IEEE MTT-S Int. Microw. Symp. Dig.*, 213–216, 2004.
9. Grigoropoulos, N., B. S. Izquierdo, and P. R. Young, "Substrate

integrated folded waveguides (SIFW) and filters," *IEEE Microw. Wireless Compon. Lett.*, Vol. 15, No. 12, 829–831, 2005.

10. Che, W. Q., L. Geng, K. Deng, and Y. L. Chow, "Analysis and experiments of compact folded substrate-integrated waveguide," *IEEE Trans. on Microw. Theory and Tech.*, Vol. 56, No. 1, 88–93, 2008.
11. Lin, H. H., "Novel folded resonators and filters," *IEEE MTT-S Int. Microw. Symp. Dig.*, 1277–1280, 2007.
12. Alotaibi, S. K. and J. S. Hong, "Novel substrate integrated folded waveguide filter," *Microw. Opt. Tech. Lett.*, Vol. 50, No. 4, 1111–1114, 2008.
13. Shen, T. M., T. Y. Huang, W. H. Wang, and R. B. Wu, "Miniaturized bandpass filters with double-folded substrate integrated waveguide resonators in LTCC," *IEEE Trans. on Microw. Theory and Tech.*, Vol. 57, No. 7, 1774–1782, 2009.
14. Wang, R., L.-S. Wu, and X.-L. Zhou, "Compact folded substrate integrated waveguide cavities and bandpass filter," *Progress In Electromagnetics Research*, Vol. 84, 135–147, 2008.
15. Shen, T. M., T. Y. Hung, and R. B. Wu, "Design of a vertically stacked substrate integrated folded-waveguide resonator filter in LTCC," *Asia-Pacific Microwave Conference*, 1–4, 2007.
16. Chen, C.-Y. and C.-C. Lin, "The design and fabrication of a highly compact microstrip dual-band bandpass filter," *Progress In Electromagnetics Research*, Vol. 112, 299–307, 2011.
17. Kuo, J.-T. and S.-W. Lai, "New dual-band bandpass filter with wide upper rejection band," *Progress In Electromagnetics Research*, Vol. 123, 371–384, 2012.
18. Zhang, X. Y., C. H. Chan, Q. Xue, and B. J. Hu, "Dual-band bandpass filter with controllable bandwidths using two coupling paths," *IEEE Microw. Wireless Compon. Lett.*, Vol. 20, No. 11, 616–618, 2010.
19. Dai, G. L., Y. X. Guo, and M. Y. Xia, "Dual-band bandpass filter using parallel short-ended feed scheme," *IEEE Microw. Wireless Compon. Lett.*, Vol. 20, No. 6, 325–327, 2010.
20. Song, K., Y. Mo, Y. Xia, S. Hu, and Y. Fan, "Compact dual-passband filter using spiral resonators," *Progress In Electromagnetics Research Letters*, Vol. 34, 187–195, 2012.
21. Yang, R. Y., K. Hon, C. Y. Hung, and C. S. Ye, "Design of dual-band bandpass filters using a dual feeding structure and embedded uniform impedance resonators," *Progress In Electromagnetics Research*, Vol. 105, 93–102, 2010.

22. Ma, D., Z. Y. Xiao, L. Xiang, X. Wu, C. Huang, and X. Kou, "Compact dual-band bandpass filter using folded SIR with two stubs for WLAN," *Progress In Electromagnetics Research*, Vol. 117, 357–364, 2011.
23. Zhou, L., S. Liu, H. F. Zhang, X.-K. Kong, and Y.-N. Guo, "Compact dual-band bandpass filter using improved split ring resonators based on stepped impedance resonator," *Progress In Electromagnetics Research Letters*, Vol. 23, 57–63, 2011.
24. Chen, W.-Y., M.-H. Weng, S.-J. Chang, H. Kuan, and Y.-H. Su, "A new tri-band bandpass filter for GSM, WiMAX and ultra-wideband responses by using asymmetric stepped impedance resonators," *Progress In Electromagnetics Research*, Vol. 124, 365–381, 2012.
25. Chiou, Y.-C. and J.-T. Kuo, "Planar multiband bandpass filter with multimode stepped-impedance resonators," *Progress In Electromagnetics Research*, Vol. 114, 129–1441, 2011.
26. Chen, X. P., K. Wu, and Z. L. Li, "Dual-band and triple-band substrate integrated waveguide filters with Chebyshev and quasi-elliptic responses," *IEEE Trans. on Microw. Theory and Tech.*, Vol. 55, No. 12, 2569–2578, 2007.
27. Chen, B. J., T. M. Shen, and R. B. Wu, "Dual-band vertically stacked laminated waveguide filter design in LTCC technology," *IEEE Trans. on Microw. Theory and Tech.*, Vol. 57, No. 6, 1554–1562, 2009.
28. Shen, W., W. Y. Yin, and X. W. Sun, "Miniaturized dual-band substrate integrated waveguide filter with controllable bandwidths," *IEEE Microw. Wireless Compon. Lett.*, Vol. 21, No. 8, 418–420, 2011.
29. Wang, R., X. L. Zhou, and L. S. Wu, "A folded substrate integrated waveguide cavity filter using novel negative coupling," *Microw. Opt. Tech. Lett.*, Vol. 51, No. 3, 866–871, 2009.
30. Hong, J. S. and M. J. Lancaster, *Microstrip Filters for RF/Microwave Applications*, J. Wiley & Sons Inc., New York, 2001.
31. Amari, S., U. Rosenberg, and J. Bornemann, "Adaptive synthesis and design of resonator filters with source/load-multi-resonator coupling," *IEEE Trans. on Microwave Theory and Tech.*, Vol. 50, No. 8, 1969–1978, 2002.